

## Seismic inversion for a smooth velocity model using a wave to diffusion transform

Rune Mittet, EMGS

### SUMMARY

Non-linear seismic inversion faces difficulties with multiple local minima due to cycle skipping. It is possible to demonstrate that cycle skipping is unlikely to appear in the diffusive domain with a very common definition of the error functional. Seismic data can be transformed to the diffusive domain and inverted to obtain an intermediate estimates of the velocity model. This intermediate velocity model may serve as initial model for inversion processing in the wave domain or may serve as a velocity model for reverse time migration.

One of the properties of the wave to diffusion transform is that it effectively extracts refractions from a common shot gather or common receiver gather containing reflections, diffractions and refractions.

### INTRODUCTION

Non-linear seismic inversion faces difficulties with multiple local minima due to cycle skipping. Several strategies are proposed to mitigate this problem. One option is to initiate the inversion with very low frequencies, of the order of 1 Hz, and then add higher frequencies at later iterations (Sirgue and Pratt, 2004). A problem, in the marine case, is that pressure amplitudes due to an airgun are small at 1 Hz. The sensors must also be sufficiently sensitive in the low frequency regime.

A second option is to apply transform methods to standard seismic data (Shin and Cha, 2009) with the purpose of getting a smooth initial model in place that roughly accounts for the traveltimes. An interesting approach for initial model estimation, based on wavefield transforms, was proposed by Virieux et al. (2012). The idea is to use a wave-to-diffusion transform on both observed and predicted data. Actually, such a transform can be used to obtain diffusive electromagnetic fields from an electromagnetic wave simulation (Lee et al., 1989). Maaø (2007) and Mittet (2010) show that this approach is numerically efficient for modeling marine controlled source electromagnetic (MCSEM) data. Virieux et al. (2012) took the approach as far as transforming a seismic shot gather to a diffusive shot gather and by that exposing the simplification of the data in the transformed time domain. Here I take this idea one step further and test it in an inversion setting. I will do this MCSEM style, thus in the frequency domain.

One of the properties of the wave-to-diffusion transform is that it effectively extracts refractions from a common shot gather or common receiver gather containing reflections, diffractions and refractions. This is explained in detail in Mittet (2015) and is a main motivation for testing it out in an inversion approach. A second property of the transform is that the field spectrum in the transformed, diffusive, domain is fairly insensitive to the propagating waveform (Mittet, 2010). Hence, this approach to the inversion of dominantly refraction data can be performed

on data generated with a standard airgun array. A third important fact is that cycle skipping is not a problematic issue in the diffusion domain. The phase is closely linked to the amplitude loss since the real and the imaginary part of the wavenumber are of similar size. It is possible to demonstrate that cycle skipping is unlikely to appear in the diffusive domain with the type of error functional used for the scheme discussed here.

### THEORY

The actual implementation is based on two transforms. The standard Fourier transform is,

$$\psi(\omega) = \int_0^T dt \psi(t) e^{i\omega t}, \quad (1)$$

where  $T$  is the duration of the shot record and  $\omega$  is angular frequency. The wave-to-diffusion transform is,

$$\psi'(\omega) = \psi(\omega') = \int_0^T dt \psi(t) e^{i\omega' t}, \quad (2)$$

where the complex transform frequency is,  $\omega' = (1+i)\sqrt{\omega\omega_0}$ . Here  $\omega_0$  is a free scaling parameter, the only requirement is that it must be positive and larger than zero. A practical value for the system discussed here is  $\omega_0 = \frac{1}{2}$  Hz. For simplicity, a constant density,  $\rho_0$ , is assumed in the following. The wave equation is for the volumetric stress,  $\sigma(\mathbf{x}, t) = -P(\mathbf{x}, t)$ , where  $P(\mathbf{x}, t)$  is the pressure at position  $\mathbf{x}$  for time  $t$ ,

$$\nabla^2 \sigma(\mathbf{x}, t) - \kappa(\mathbf{x}) \partial_t^2 \sigma(\mathbf{x}, t) = S(\mathbf{x}, t), \quad (3)$$

where  $\kappa(\mathbf{x})$  the compliance and  $S(\mathbf{x}, t)$  is a source term. The inversion parameter will be compliance. The relation to velocity,  $c(\mathbf{x})$ , is simply,  $c(\mathbf{x}) = [\rho_0 \kappa(\mathbf{x})]^{-\frac{1}{2}}$ . A standard Fourier transform of equation 3 gives the equation,

$$\nabla^2 \sigma(\mathbf{x}, \omega) + \omega^2 \kappa(\mathbf{x}) \sigma(\mathbf{x}, \omega) = S(\mathbf{x}, \omega), \quad (4)$$

whereas by using the wave-to-diffusion transform in equation 2,

$$\nabla^2 \sigma'(\mathbf{x}, \omega) + i\omega \kappa(\mathbf{x}) \sigma'(\mathbf{x}, \omega) = S'(\mathbf{x}, \omega). \quad (5)$$

The Fréchet derivative for the wave equation, equation 4, is

$$\mathcal{F}(\mathbf{x}; \mathbf{x}_r, \omega | \mathbf{x}_s) = \omega^2 \Delta V(\mathbf{x}) G(\mathbf{x}, \omega | \mathbf{x}_r) \sigma(\mathbf{x}, \omega | \mathbf{x}_s), \quad (6)$$

where  $\mathbf{x}_s$  and  $\mathbf{x}_r$  are source and receiver positions respectively.  $\Delta V(\mathbf{x})$  is the cell volume. The Fréchet derivative for the diffusion equation, equation 5, is

$$\mathcal{F}'(\mathbf{x}; \mathbf{x}_r, \omega | \mathbf{x}_s) = i\omega \Delta V(\mathbf{x}) G'(\mathbf{x}, \omega | \mathbf{x}_r) \sigma'(\mathbf{x}, \omega | \mathbf{x}_s). \quad (7)$$

For both types of transforms the data error part of the error functional has the same form,

$$\epsilon^D = \sum_{\omega, \mathbf{x}_r, \mathbf{x}_s} = \frac{[\Delta \sigma(\mathbf{x}_r, \omega | \mathbf{x}_s)]^* [\Delta \sigma(\mathbf{x}_r, \omega | \mathbf{x}_s)]}{[\delta \sigma(\mathbf{x}_r, \omega | \mathbf{x}_s)]^2} \quad (8)$$

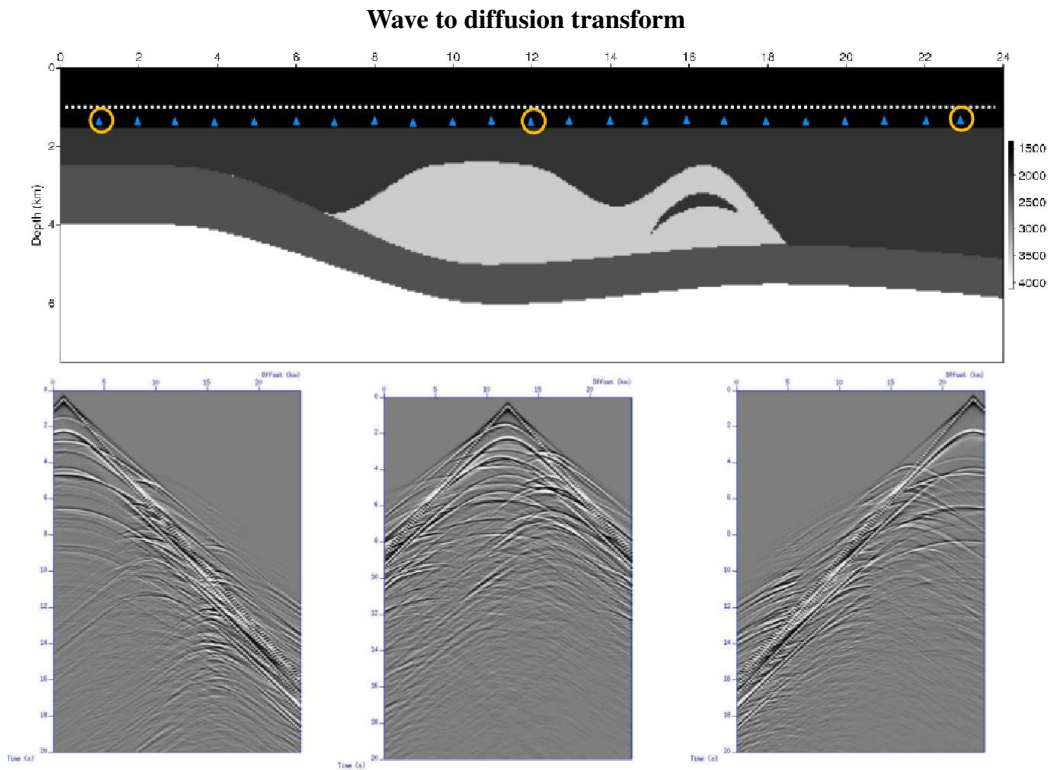


Figure 1: The true model and 3 common receiver gathers. The shot positions are marked with white dots. The receiver positions are marked with blue triangles. An orange ring marks the 3 receivers for which data are plotted.

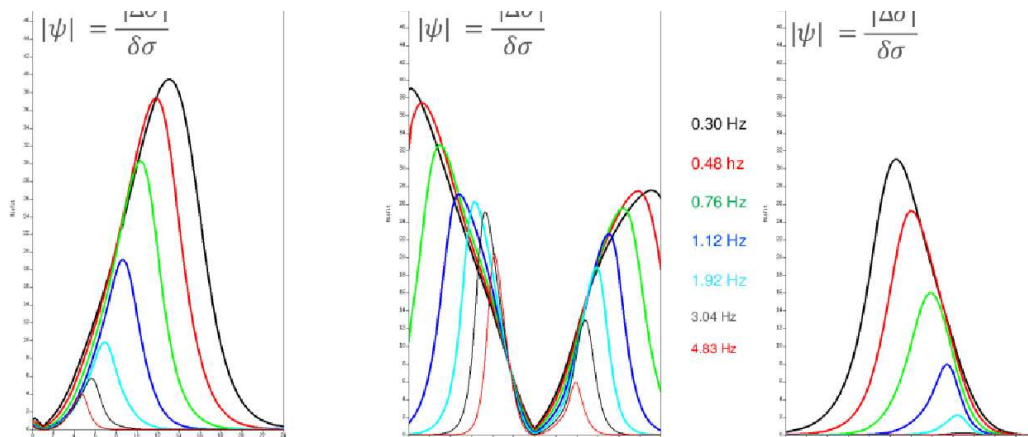


Figure 2: Data misfit functions in the transformed domain. The misfit functions are normalized by the data uncertainties and are kernels for the error functional.

where the  $*$  denotes complex conjugate and the misfit between observed and predicted data is

$$\Delta\sigma(\mathbf{x}_r, \omega|\mathbf{x}_S) = \sigma^{Obs}(\mathbf{x}_r, \omega|\mathbf{x}_S) - \sigma^{Prd}(\mathbf{x}_r, \omega|\mathbf{x}_S). \quad (9)$$

The data uncertainty model is as discussed in Mittet and Morten (2012),

$$\delta\sigma(\mathbf{x}_r, \omega|\mathbf{x}_S) \approx \sqrt{\gamma^2 |\sigma^{Obs}(\mathbf{x}_r, \omega|\mathbf{x}_S)|^2 + \eta^2}, \quad (10)$$

where  $\gamma$  is a multiplicative uncertainty factor of order 1 percent and where  $\eta$  is the ambient noise level.

The data part of the inversion is well defined as we have expressions for the data misfit, the data uncertainty and the Fréchet derivatives. The model space part of the error functional is a mild horizontal smoothing. The update for the compliance is based on a Gauss-Newton trust-region method. The wave equation (equation 3) is solved in the time domain. For diffusion domain inversion the transform in equation, 2 is applied to the observed data, the predicted data and the calculation of Green's functions. The Fréchet derivative is from equation 7.

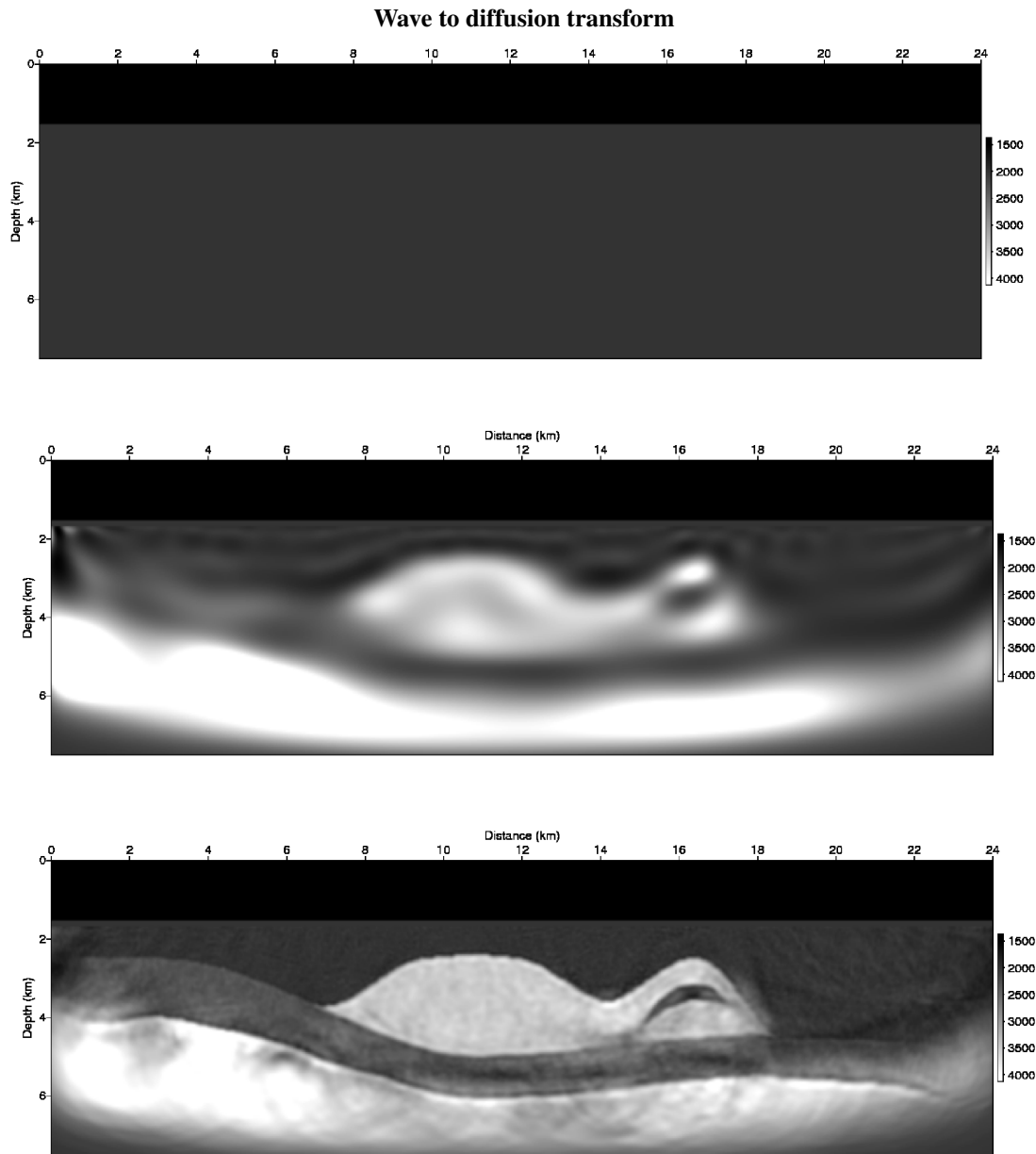


Figure 3: From top to bottom: The initial halfspace model. The intermediate model obtained by inversion in the transformed domain. The final model obtained by inversion in the frequency domain starting from the intermediate model.

For the wave domain inversion the transform in equation 1 is applied to the observed data, the predicted data and the calculation of Green's functions. The Fréchet derivative is from equation 6. Thus, a simple switch selects between the two approaches, almost all the inversion code is common for the two schemes.

## RESULTS

The true model is displayed in Figure 1. The shot positions are marked with white dots. The receiver positions are marked with blue triangles. The shot separation is 200 m and the re-

ceiver separation is 1 km. Inversion is first performed in the diffusive domain using 7 log-spaced frequencies. The transform in equation 2 is complex and has an exponential damping term. The product of the field and the exponential damping term at the final recording time,  $T$  must be close to zero. Thus, the lowest allowable frequency in the diffusive domain is a function of the total recording time,

$$f \geq \frac{1}{2\pi\omega_0} \left( \frac{\ln(\varepsilon)}{T} \right)^2, \quad (11)$$

where  $\varepsilon$  is a small number. The values  $\varepsilon = 1 \times 10^{-6}$ ,  $\omega_0 = \frac{1}{2}$  Hz and  $T = 20$  s as used here gives a lower limit of 0.15 Hz.

## Wave to diffusion transform

The highest useful frequency is given by the same formula as equation 11 but with  $T$  replaced by  $T'$  where  $T'$  is the time where the first refraction clearly separates from the first reflections. For the configuration used here we find  $T' \approx 2$  s and hence an upper limit of 15 Hz. For the inversion the 7 frequencies ranged from 0.3 Hz to 4.8 Hz.

The initial model is a halfspace with velocity 2000 m/s in the formation. The misfit normalized by the data uncertainty for the first iteration is shown in Figure 2. The behavior is very similar to MCSEM data (Mittet and Morten, 2012). The initial halfspace model is shown at the top of Figure 3. The result of the inversion in the diffusive domain is shown in the middle of Figure 3. The result is smooth but indications of the low velocity inclusion at “Distance” 16 km and “Depth” 3 km is present.

The final inversion is performed in the wave domain. The initial model for the wave domain inversion is the final model from the diffusive domain inversion. Nine equally spaced frequencies from 1 to 9 Hz were used in this inversion. Several attempts were made, starting the inversion directly in the wave domain and from a half-space model. Different sets of frequencies were tested including sequential single frequency inversions starting at 1 Hz. All final models were inferior to the final model in Figure 3. A more sophisticated wave-domain inversion scheme, with targeted preprocessing of the input data, may make it possible to go all the way from the half-space model to the final model in Figure 3 directly in the wave domain. The requirement for data preprocessing, if the inversion is started in the diffusive domain, is that noise prior to the first arrival is muted. No muting after the first arrival is required, the wave-to-diffusion transform does an effective job in extracting the refractions.

### CYCLE-SKIPPING EFFECTS

The robustness of the diffusive domain inversion with respect to the halfspace initial model is largely due to the fact that the wave-to-diffusion transform is effective in extracting refractions as compared to reflections from a common shot or common receiver gather. It is also worth noting that cycle-skipping effects behave differently in the diffusive domain as compared to the wave domain. Cycle-skipping effects are less common in the diffusive domain even for relatively high frequencies. The reason is that there is a close relationship between amplitude and traveltimes in the diffusive domain since the wavenumber has equal real and imaginary part. A certain amount of phase shift due to propagation also implies a certain amount of exponential damping. This relationship does not exist in the wave domain where the wavenumber is real.

A rough explanation follows: Assume that the observed and predicted field can be described by,

$$\begin{aligned} D^{Obs} &= A^{Obs} e^{i\phi^{Obs}}, \\ D^{Prd} &= A^{Prd} e^{i\phi^{Prd}}. \end{aligned} \quad (12)$$

and that the amplitude factors account for source strength and

transmission and reflection effects between source and receiver. The phase factor accounts for the propagation effects (time delay) between source and receiver. The kernel of the error functional has the form,

$$\varepsilon = (D^{Obs} - D^{Prd})^* (D^{Obs} - D^{Prd}). \quad (13)$$

To keep the argument simple I further assume that the amplitude factors are approximately equal, that is  $A^{Obs} \approx A^{Prd} \approx A$ . The main contribution to the error functional does come from misfits in traveltimes in this case,

$$\varepsilon \approx |A|^2 [(e^{i\phi^{Obs}} - e^{i\phi^{Prd}})^2 ((e^{i\phi^{Obs}} - e^{i\phi^{Prd}}))], \quad (14)$$

which simplifies to,

$$\varepsilon \approx 2|A|^2 [1 - \cos(\phi^{Obs} - \phi^{Prd})] = 2|A|^2 [1 - \cos(\Delta\phi)], \quad (15)$$

with  $\Delta\phi = \phi^{Obs} - \phi^{Prd}$ . The error functional is degenerate in this case with multiple zeroes for  $\Delta\phi = 0 \pm 2\pi n$  with  $n \geq 1$ .

In the diffusive domain we have that the real and imaginary parts of  $\phi$  have equal size,  $\phi = (1+i)\beta$ . Under the assumption that the amplitude factors are approximately equal we have,

$$\varepsilon \approx |A|^2 [(e^{i(1+i)\beta^{Obs}} - e^{i(1+i)\beta^{Prd}})^2 ((e^{i(1+i)\beta^{Obs}} - e^{i(1+i)\beta^{Prd}}))], \quad (16)$$

which simplifies to,

$$\varepsilon \approx 2|A|^2 e^{-(\beta^{Obs} + \beta^{Prd})} [\cosh(\beta^{Obs} - \beta^{Prd}) - \cos(\beta^{Obs} - \beta^{Prd})], \quad (17)$$

or,

$$\varepsilon \approx 2|A|^2 e^{-(\beta^{Obs} + \beta^{Prd})} [\cosh(\Delta\beta) - \cos(\Delta\beta)] \quad (18)$$

with  $\Delta\beta = \beta^{Obs} - \beta^{Prd}$ . The error functional is not degenerate in this case since the hyperbolic cosine is equal to unity for zero argument and larger than unity elsewhere. The error functional can only approach zero if  $\Delta\beta = 0$ .

### CONCLUSIONS

Seismic data can be transformed to the diffusive domain and inverted to obtain intermediate estimates of the velocity model. This intermediate velocity model may serve as initial model for inversion processing in the wave domain or may serve as a velocity model for reverse time migration.

The shape of the wavefield spectrum in the diffusive domain is fairly insensitive to the shape of the wavefield spectrum in the wave domain. Thus, standard airgun data can be used for this type of diffusive inversion. There is no direct need for a specialized source. However, a low frequency source may give a somewhat better signal to noise ratio also in the diffusive domain.

## REFERENCES

- Lee, K. H., G. Liu, and H. F. Morrison, 1989, A new approach to modeling the electromagnetic response of conductive media: *Geophysics*, **54**, 1180–1192, <https://doi.org/10.1190/1.1442753>.
- Maaø, F. A., 2007, Fast finite-difference time-domain modeling for marine-subsurface electromagnetic problems: *Geophysics*, **72**, no. 2, A19–A23, <https://doi.org/10.1190/1.2434781>.
- Mittet, R., 2010, High-order finite-difference simulations of marine CSEM surveys using a correspondence principle for wave and diffusion fields: *Geophysics*, **75**, no. 1, F33–F50, <https://doi.org/10.1190/1.3278525>.
- Mittet, R., 2015, Seismic wave propagation concepts applied to the interpretation of marine controlled-source electromagnetic: *Geophysics*, **80**, no. 2, E63–E81, <https://doi.org/10.1190/geo2014-0215.1>.
- Mittet, R., and J. P. Morten, 2012, Detection and imaging sensitivity of the marine CSEM method: *Geophysics*, **77**, no. 6, E411–E425, <https://doi.org/10.1190/geo2012-0016.1>.
- Shin, C., and Y. H. Cha, 2009, Waveform inversion in the Laplace-Fourier domain: *Geophysical Journal International*, **177**, 1067–1079, <https://doi.org/10.1111/j.1365-246x.2009.04102.x>.
- Sirgue, L., and G. Pratt, 2004, Efficient waveform inversion and imaging: A strategy for selecting temporal frequencies: *Geophysics*, **69**, 231–248, <https://doi.org/10.1190/1.1649391>.
- Virieux, J. M., R. Brossier, S. Garambois, S. Operto, and A. Ribodetti, 2012, Making seismic data as CSEM data through the Backlund transform: 5th Saint Petersburg International Conference and Exhibition, <https://doi.org/10.3997/2214-4609.20143635>.